Zero Kinetic Energy Photoelectron Spectroscopy of Pyrene

ARTICLE *in* THE JOURNAL OF PHYSICAL CHEMISTRY A · OCTOBER 2010

Impact Factor: 2.69 · DOI: 10.1021/jp1024813 · Source: PubMed

Zero Kinetic Energy Photoelectron Spectroscopy of Pyrene†

Jie Zhang, Fangyuan Han, and Wei Kong*

Department of Chemistry, Oregon State University, Corvallis, Oregon 97331-4003

Received: March 19, 2010; Revised Manuscript Received: July 2, 2010

We report zero kinetic energy photoelectron (ZEKE) spectroscopy of pyrene via resonantly enhanced multiphoton ionization. Our analysis centers on the symmetry of the first electronically excited state (S_1), its vibrational modes, and the vibration of the ground cationic state (D_0). From comparisons between the observed vibrational frequencies and those from ab initio calculations at the configuration interaction singles level using the 6-311G (d,p) basis set, and based on other previous experimental and theoretical reports, we confirm the $^1B_{2u}$ symmetry for the S_1 state. This assignment represents a reversal in the energy order of the two closely spaced electronically excited states from our theoretical calculation, and extensive configuration interactions are attributed to this result. Among the observed vibrational levels of the S_1 state, three are results of vibronic coupling due to the nearby second electronically excited state. The ZEKE spectroscopy obtained via the vibronic levels of the S_1 state reveals similar modes for the cation as those of the intermediate state. Although we believe that the ground ionic state can be considered a single electron configuration, the agreement between theoretical and experimental frequencies for the cation is limited. This result is somewhat surprising based on our previous work on cata-condensed polycyclic aromatic hydrocarbons and small substituted aromatic compounds. Although a relatively small molecule, pyrene demonstrates its nonrigidity via several out-of-plane bending modes corresponding to corrugation of the molecular plane. The adiabatic ionization potential of neutral pyrene is determined to be 59 888 ± 7 cm^{-1}.

Introduction

Polycyclic aromatic hydrocarbons (PAHs), also known as polyarenes, are hydrocarbon compounds consisting of more than two fused aromatic rings without any heteroatoms or substituents. In the arena of fundamental chemistry and physics, PAHs are an interesting group of molecules: the hexagonal linkages of the carbon atoms in PAHs determine their high geometric symmetry, and the delocalization of π electrons has played an important role in the development of the Hückel theory.[1] From a practical point of view, atmospheric PAHs are formed during incomplete combustion of fossil fuels, garbage, or other organic substances like tobacco or charbroiled meat, hence they are also related to environmental toxicity[2] and carcinogenicity.[3−5] More recently, PAHs have gained further interests because of their connection and application in molecular engineering of electronic devices.[6,7] In astrophysics and particularly in studies of the interstellar medium (ISM),[8,9] these carbon abundant molecules have been suggested to be potentially related to the origin of life via the formation of primitive organic molecules including amino acids in the pre-DNA world.[10−12] In addition, neutral and ionic PAHs are considered promising candidates for the interstellar absorption and emission bands, including the unidentified infrared (UIB) emission bands.[13−19]

Spectroscopic identification of individual PAH molecules requires unique fingerprints of each molecule. Although all PAHs have common structural features and hence common spectroscopic signatures, particularly in the mid-infrared (MIR), the unique fingerprint of each individual molecule lies in the far-infrared (FIR). This is because MIR modes are mostly representative of local functional groups, while FIR modes are representative of the skeletal motions of the whole molecular frame.[20−22] Consequently, although many studies have been devoted to MIR spectroscopy of neutral and charged PAHs,[23−28] no specific PAH molecule has been identified yet in the ISM. Moreover, PAH cations are speculated to be even more probable candidates as carriers of UIBs than their neutral counterparts.[20,29] Hence, FIR spectroscopy of PAH cations is instrumental in mapping out the chemical composition of the ISM.

The technique of zero kinetic energy photoelectron (ZEKE) spectroscopy offers an indirect solution to this challenge in astrophysics.[30] ZEKE is known for its high resolution of cation rovibrational spectroscopy. The high Rydberg states in ZEKE are longer lived when they are associated with lower vibronic states of the cation, which makes it particularly suitable for studies of lower frequency vibrational modes. Thus, by detecting electrons from pulsed field ionization in ZEKE spectroscopy, we can avoid both the light source and the detector problems in typical FIR and submillimeter wave experiments. The vibrational information from ZEKE is largely governed by the Franck−Condon principle, hence the information from ZEKE might not be directly applicable for line identification in astronomy. However, as we have demonstrated in pentacene,[31] vibronic coupling can probe some IR active modes. In addition, by offering measurements of several IR forbidden modes, ZEKE can serve as an experimental calibration method for the active bands in the FIR. Moreover, IR forbidden modes are relevant to the modeling of the energy balance in the interstellar medium and to the modeling of PAH emissions with high internal temperatures.[32−36] Hence, ZEKE offers complementary information to and fills the gap in techniques of single photon absorption or emission.[23,37−40]

PAHs can be classified into two groups: acenes and phenes. Acenes are cata-condensed (cata-fused) PAHs in which no carbon atom is shared by more than two rings. Phenes are peri-

† Part of the "Klaus Müller-Dethlefs Festschrift".

* To whom correspondence should be addressed. E-mail: wei.kong@oregonstate.edu. Fax: 541-737-2062.

10.1021/jp1024813
Published on Web 08/02/2010

condensed PAHs in which at least one carbon atom is shared by three rings.[5] There have been several reports of ZEKE spectroscopy of small cata-condensed PAHs including naphthalene, anthracene, tetracene, and pentacene.[31,41−43] In our studies of tetracene and pentacene, we have observed total symmetric a_g modes allowed by the Franck−Condon principle, and IR active modes through vibronic coupling.[31,43] Pyrene is a peri-condensed PAH molecule. Its first two electronically excited states have been widely studied both experimentally and theoretically in the gas phase and in the condensed phase.[44−49] The infrared spectroscopy of neutral pyrene is also thoroughly studied in rare gas matrices, solid state, and gas phase.[50] However, not much information of the cation in the FIR region has been revealed yet, although many works have been devoted to the MIR and near-IR region (NIR),[23,37−40] ranging from 500 to 3000 cm^{-1}. In this paper, we report two-color two photon REMPI and ZEKE spectroscopy of pyrene. We present detailed spectroscopic analysis for the vibrational levels of the first electronically excited state (S_1) and the ground cationic state (D_0). Additional insights can be obtained from the results of ab initio and density functional calculations. Structural changes due to electronic excitation and ionization will be elucidated from the observed active vibrational modes and from comparisons between the REMPI and ZEKE spectra.

Experimental Setup

The experimental apparatus is a standard molecular beam machine with a differentially pumped high vacuum system and a time-of-flight mass spectrometer, which can be converted into a pulsed field ionization zero kinetic energy photoelectron spectrometer.[43] The sample pyrene (Aldrich) was housed and heated to 160 °C in the nozzle to obtain sufficient vapor pressure. The vapor was seeded in 3 atm of argon and expanded into vacuum through a pulsed valve with a 1 mm orifice. The laser systems for the REMPI experiment included a Nd:YAG (Precision II 8000, Continuum) pumped optical parametric oscillator (OPO, Panther, Continuum) and a Nd:YAG (Spectra Physics, GCR 230) pumped dye laser (Laser Analytical Systems, LDL 2051). The pump laser in the 354−370 nm range, with a bandwidth of 0.3 cm^{-1} obtained from the frequency-doubled dye laser system, had a pulsed energy of 1.5 mJ/pulse. The ionization laser in the 300−315 nm range with a bandwidth of 1.3 cm^{-1} from the frequency-doubled output of the OPO system had a pulse energy of 0.5 mJ/pulse. The absolute wavelength of each laser was calibrated using an iron hollow-cathode lamp filled with neon. The pump laser and ionization laser were set to counter-propagate, and the light path, the flight tube, and the molecular beam were mutually perpendicular. The relative timing among the three laser pulses was controlled by two delay generators (Stanford Research, DG 535), and the optimal signal was obtained under temporal overlap between the pump and ionization lasers. In the ZEKE experiment, molecules excited to high Rydberg states were allowed to stay for 1−2 μs in the presence of a constant DC spoiling field of ~1 V/cm, after which ionization and extraction were achieved by a pulsed electric field of ~5 V/cm.

Gaussian 03 suite[51] was used to optimize the molecular structure and to obtain vibrational frequencies for assignment of the observed vibronic structures from REMPI and ZEKE. For the ground state of the neutral and the cationic state, density functional theory (DFT) calculations using the B3LYP functional were performed with the 6-311G (d,p) basis set. For the excited electronic states, configuration interaction singles (CIS) with the 6-311G (d,p) basis set was used. This choice was dictated by the size of the molecule and by our computational resources. In addition, we have also used the same method for other PAHs and a few benzene derivatives with satisfactory results.[31,43,52−56] The vibrational frequencies from our CIS calculation were scaled by a factor of 0.9245, the choice of which will be discussed in the following section. For the D_0 state, a scaling factor of 0.995 was adopted.

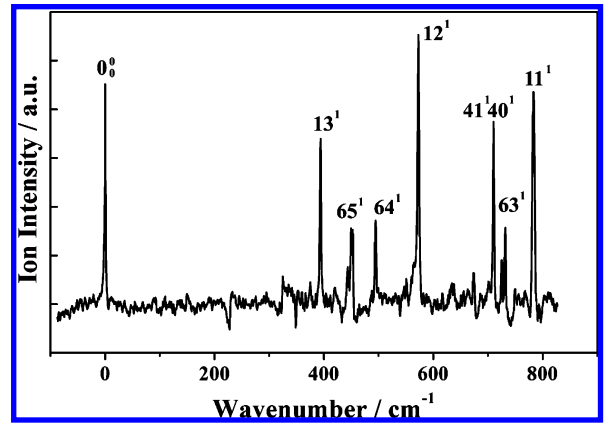

Figure 1. (1 + 1′) REMPI spectrum of jet-cooled pyrene. The spectrum is shifted by 27 211 cm^{-1} (the origin of the $S_1 \leftarrow S_0$ transition) to emphasize the frequencies of the different vibrational levels of the S_1 state.

TABLE 1: Observed and Calculated Vibrational Frequencies of the S_1 State of Pyrene

experiment	calculation[a]	assignment	symmetry
394	392	13^1	a_g
450	448	65^1	b_{3g}
495	501	64^1	b_{3g}
573	567	12^1	a_g
712	718	$40^1 41^1$	b_{1g}
732	729	63^1	b_{3g}
783	788	11^1	a_g

[a] A scaling factor of 0.9245 is included in the calculation result.

Results

Two-Color 1 + 1′ REMPI Spectroscopy. The two-color 1 + 1′ REMPI spectrum of pyrene near the origin of the $S_1 \leftarrow S_0$ electronic transition is displayed in Figure 1. The ionization laser was set at 280 nm and was temporally overlapped with the scanning resonant laser. The intense peak at 27211 cm^{-1} is assigned as the origin band, and the other observed vibronic transitions are listed in Table 1. The labeling of each vibrational mode is based on spectroscopic conventions, that is, by using consecutive numbers in reference to the symmetry species and the frequency in decreasing order. Due to the fact that vibrational frequencies generated by ab initio calculations are usually too high, we used a scaling factor and adjusted its value to match the experimental results using a least-squares linear regression method. The resulting scaling factor of 0.9245 had a value of 0.9996 for the coefficient of determination (R^2). With this scaling factor, the maximum deviation between theory and experiment is 6 cm^{-1}.

Pyrene is considered planar with D_{2h} symmetry (the definition of molecular axis is shown in Figure 4[44]). Among its 72 normal modes, 13 belong to the a_g symmetry species allowed by the Franck−Condon principle in the $^1B_{2u}(S_1) \leftarrow {}^1A_g(S_0)$ transition. Within the spectral range of our experiment, the 3 lowest a_g modes are observable and are assigned as modes 13−11. Since the energy of the $^1B_{1u}$ (S_2) state is only ~4000 cm^{-1} above that

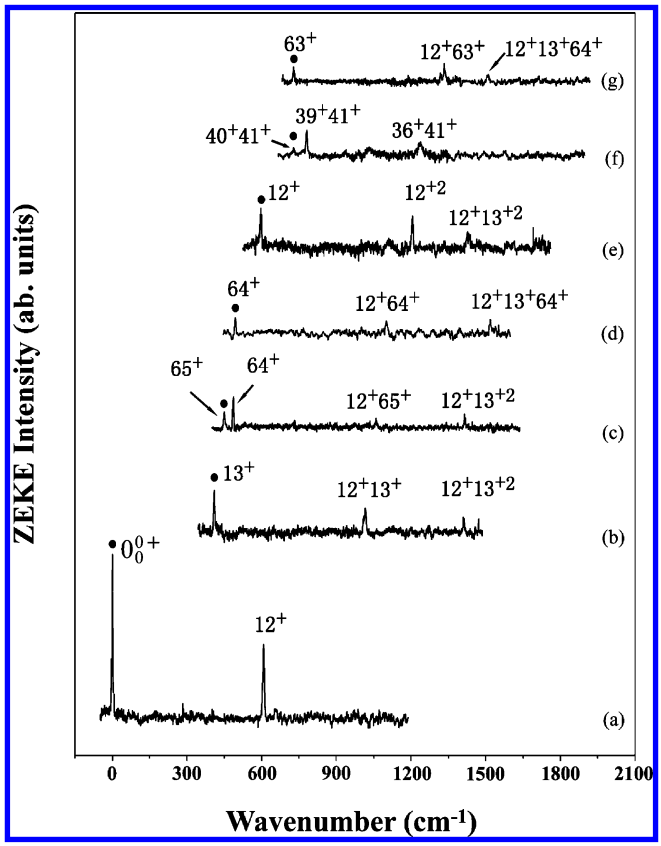

Figure 2. Two-color ZEKE spectra of pyrene recorded via seven vibrational levels of the S_1 state as intermediate states: (a) 0^0, (b) 13^1, (c) 65^1, (d) 64^1, (e) 12^1, (f) 41^140^1, and (g) 63^1. The energy in the *x*-axis is relative to the ionization threshold at 59 888 cm^{-1}. The assignment in the figure refers to the vibrational levels of the cation, and the corresponding vibrational level of the intermediate state is labeled by a black dot in each panel.

of the S_1 state in the gas phase, some Franck−Condon forbidden b_{3g} modes can be activated by Herzberg−Teller vibronic coupling. The three b_{3g} modes shown in the spectrum are assigned as modes 65−63, in agreement with the fluorescence excitation spectra by Mangle and Topp in 1986, Borisevich et al in 1995, and Baba et al in 2009.[44,45,47] However, a strong peak at 712 cm^{-1} has never been assigned before, and we think that it is most likely a combination of two b_{2g} modes, 41 and 40. On the basis of our calculation, this combination is only 6 cm^{-1} from the experimental result. This assignment will be further confirmed from ZEKE in the following section.

ZEKE Spectroscopy. By scanning the ionization laser while setting the resonant laser at one of the intermediate states identified in the above REMPI experiment, we obtained pulsed field ionization ZEKE spectra as shown in Figure 2. The assignment of the vibrational levels of the cation is noted by a superscript "+". The identity of the vibrational level of the intermediate state for each ZEKE spectrum is labeled in the corresponding panel by a black dot. The experimental and theoretical values are shown in Table 2. The calculation was performed at the B3LYP/6-311G (d,p) level. Using a least-squares fitting procedure similar to that for the S_1 state, a factor of 0.995 for the theoretical vibrational frequencies of the cation was obtained, after which the agreement between theory and experiment is reasonable. Limited by the line width of the resonant transitions and the pulsed electric field, the uncertainty of the experimental values of the ZEKE spectra is 7 cm^{-1}.

The ZEKE spectra are sparse, and each consists of no more than three peaks with similar intensities. Trace (a) was recorded

TABLE 2: Observed and Calculated Vibrational Frequencies of Pyrene Cation

intermediate level in the S_1 state							cation	
0_0^0	13_0^1	65_0^1	64_0^1	12_0^1	$40_0^141_0^1$	63_0^1	calculation[a]	assignment
0							0	origin
	410						412	13^+
		451					457	65^+
		491	494				499	64^+
608				598			598	12^+
						728	738	63^+
					732		730	40^+41^+
					781		798	39^+41^+
	1014						1010	12^+13^+
		1056					1055	12^+65^+
			1099				1097	12^+64^+
				1206			1196	12^{+2}
					1240		1246	36^+41^+
						1333	1336	12^+63^+
	1413	1415		1427			1422	12^+13^{+2}
			1519			1510	1509	$12^+13^+64^+$

[a] A scaling factor of 0.995 is included in the calculation result.

via the origin of the S_1 state, and the most intense peak corresponds to the origin of the cation. The adiabatic ionization potential is thus determined to be 59 888 ± 7 cm^{-1} (7.4064 ± 0.0007 eV), taking into account the shift caused by the pulsed electric field. This value is 155 cm^{-1} higher than that determined by Hager and Wallace[57] using two-laser photoionization in 1988. This discrepancy might be caused by the extrapolation method in the previous paper. Although the same selection rule applies to both the REMPI and the ZEKE process, only mode 12 is observed in the ZEKE spectrum from the origin of the S_1 state, while other Franck−Condon allowed and vibronic allowed bands observable in the REMPI experiment are missing in the ZEKE spectrum.

Trace (e) shows the ZEKE spectrum of pyrene taken via the in-plane breathing mode 12 of the S_1 state. In addition to the fundamental band, the second harmonic of the same mode is also observable, whereas 12^{+3} is out of range of this observation window. A few other ZEKE spectra obtained via different vibrational levels of the S_1 state also involve combinations with mode 12, including 12^+13^+, 12^+65^+, 12^+64^+, 12^+63^+, 12^+13^{+2}, and $12^+13^+64^+$. In fact, the only spectrum that does not contain a combination band with mode 12 is trace (f), obtained via the combination of two b_{2g} modes. On the other hand, no combination bands are observable in trace (e), meaning that ionization via mode 12 does not activate any other mode.

Excitations in the vibronic modes 63−65 and out-of-plane modes 40 and 41 are largely preserved during ionization, but the resulting ZEKE spectra also contain additional combinations with mode 12. Among the three in-plane twisting modes of 63−65, mode 64 is the most prevalent, observable in the ZEKE spectra obtained via the other two b_{3g} intermediate vibronic levels.

The out-of-plane b_{2g} modes are only observable from their combination bands, and preservation of the vibrational excitation during ionization is inconsistent. Trace (f) consists of three combination bands with mode 41. The vibration of the intermediate level involves modes 40 and 41, but the corresponding combination band is barely observable in the ZEKE spectrum. Instead, two higher frequency modes of the same b_{2g} symmetry are observed. The facts that all modes in the ZEKE spectrum can be assigned with confidence and that all modes are of b_{2g} symmetry further vindicate the assignment of the intermediate state.

Figure 3 shows the displacement vectors of the observed modes both in REMPI and ZEKE. All three a_g modes cor-

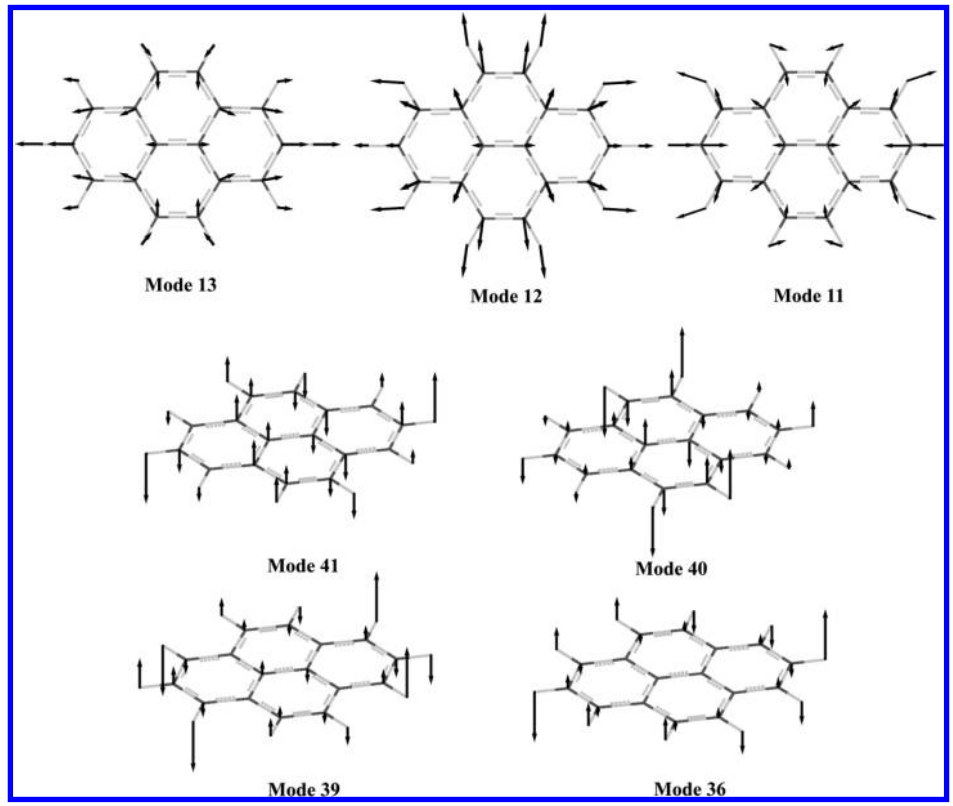

Figure 3. Displacement vectors for a few normal modes of pyrene.

respond to expansion/shrinkage of the molecular frame. In particular, mode 12 involves breathing in the vertical direction, mode 13 involves breathing in the horizontal direction, and mode 11 involves breathing of the two terminal horizontal rings. Mode 41 and mode 39 are out-of-plane waving modes along the long axis. They are similar to the b_{3g} modes we have observed in the ZEKE spectrum of pentacene.[31] If we define the length of the molecular long axis as L, the waving cycle of mode 41 is $L/2$ and that of mode 39 is $L/4$, with a wave propagation vector along the long axis. Mode 40 is characteristic of peri-condensed PAHs, and its displacement vectors involve concurrent waving along both axes in the molecular plane. Mode 36 is basically CH out-of-plane waving.

In our previous work on ZEKE spectroscopy of substituted aromatic compounds,[52−55] we have used the degree of conservation of the vibrational excitation of the intermediate state as an indicator of the stability of the molecular frame from S_1 to D_0. When the substituent is electron-rich, the cation exhibits negligible geometric change upon ionization, resulting in essentially diagonal Franck−Condon factors. The ZEKE spectra are dominated by one vibrational band corresponding to the same vibrational excitation of the intermediate S_1 state. This propensity breaks down with electron-poor substituents,[56] and the resulting ZEKE spectra contain long progressions of modes related to skeletal rearrangements. The ZEKE spectra of pyrene seem to fall in between these two cases. The multiple fused rings have a substantial ability to absorb the positive charge of the cation, but they are less efficient than an electron-rich substituent such as an amino group or a halogen atom.

Discussion

The Nature of the S_1 State. The symmetry of the S_1 state has been discussed most recently by Baba et al[47] based on fluorescence excitation and dispersed fluorescence spectra. However, some historical recount and some additional details are necessary for a comprehensive understanding. Our CIS calculation using the 6-311G(d,p) basis set has resulted in two closely spaced electronically excited states $^1B_{1u}$ and $^1B_{2u}$. The energy order of the two states, however, is questionable. In previously reported calculations,[46,49] the $^1B_{2u}$ state had a fairly weak oscillator strength with a transition dipole along the short axis, while the $^1B_{1u}$ state had an oscillator strength 2−3 orders larger than that of the $^1B_{2u}$ state, and its transition dipole was along the long axis. In Tanaka's work of electronic absorption of crystalline pyrene,[48] four excited states were reported. Further polarized excitation revealed that the S_1 state had a transition dipole along the short axis, and the second excited state, about 3000 cm^{-1} higher in energy, had a transition dipole along the long axis. The oscillator strength of the second state was also determined to be 2 orders of magnitude greater than that of the first one. These experimental results indicate that the $^1B_{2u}$ state should be the lowest singlet excited state S_1, while the $^1B_{1u}$ state should be the S_2 state. However, this order is opposite to most theoretical results obtained using different computational methods.[46,49] For example, Bito, Shida and Toru used four different methods,[49] and only two resulted in $^1B_{2u}$ for S_1, and only MRSD-CI (multireference singles and doubles − configuration interaction) yielded both the same order and similar excitation energies as those from Tanaka[48] for the two excited states. The TDDFT (time-dependent DFT) method was also evaluated by Dierksen and Grimme,[46] and the resulting order of states was opposite to that of Tanaka.[48] Our calculation at the [CIS/6-311G(d,p)] level resulted in a lower $^1B_{1u}$ state than a $^1B_{2u}$ state, again opposite to the experimental order of Tanaka.[48]

We then further compared the vibrational frequencies of the two electronic states with our experimental results from Table 1, taking into consideration that the experimental uncertainty in the transition frequencies is less than 3 cm^{-1} for the one-

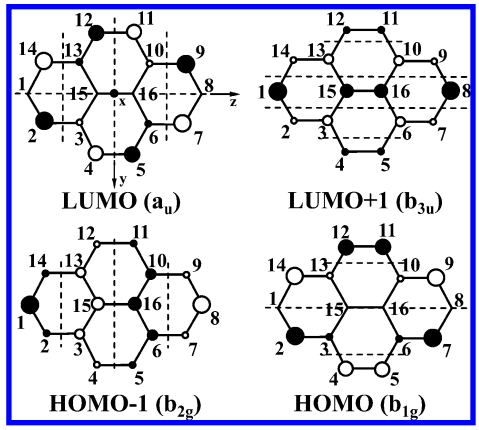

Figure 4. The HOMO − 1, HOMO, LUMO and LUMO + 1 of pyrene. The dashed lines mark the nodal planes based on a simple Hückel calculation. The definition of the molecular coordinate system is also shown.

photon resonant REMPI experiment. For the $^1B_{2u}$ state, the corresponding R^2 value was 0.9996 with a maximum deviation of 6 cm^{-1}. On the other hand, for the $^1B_{1u}$ state using the least-squares fitting procedure, a single scaling factor fit resulted in a R^2 value of 0.9889 and a maximum deviation of 23 cm^{-1}. If we choose to use two different scaling factors for the a_g and b_{3g} modes from the $^1B_{1u}$ state, an equally satisfactory comparison as that of Table 1 can also be achieved. In fact, Baba et al[47] did adopt two different scaling factors and rationalized their choice by invoking different interactions between the electronic states. However, if one scaling factor from the $^1B_{2u}$ state can achieve the same level of agreement as that with two scaling factors from the $^1B_{1u}$ state, it seems rational to adopt the choice of the former $^1B_{2u}$ symmetry. Although the value of a scaling factor cannot be used to support the assignment of an electronic state, its inconsistency for all vibrational bands should be indicative of possible problems.

The molecular orbitals and energy level distribution from CIS/6-311G(d,p) are very similar to those from simple Hückel calculations, and for clarity, the relevant HOMO (−1) and LUMO (+1) orbitals from simple Hückel calculations are reproduced in Figure 4 together with the numbering scheme of the carbon atoms and the definition of molecular axis. Both HOMO and HOMO − 1 have three nodal planes, and both LUMO and LUMO + 1 have four nodal planes. The transition dipoles of LUMO ← HOMO and LUMO + 1 ← HOMO − 1 are $b_{1g} \times a_u = b_{1u}$ and $b_{2g} \times b_{3u} = b_{1u}$, both in the direction of the long axis, while those of the nearly degenerate pair LUMO ← HOMO − 1 and LUMO + 1 ← HOMO are $b_{2g} \times a_u = b_{2u}$ and $b_{1g} \times b_{3u} = b_{2u}$, with transition dipoles in the vertical direction along the short axis. The energies of both the vertical and horizontal transitions are similar, as implied by the distribution of nodal planes in the MOs. On the basis of the work of Callis,[58] the horizontal transitions are L_a in nature with B_{1u} symmetry, and the vertical transitions are L_b in nature with B_{2u} symmetry. The reversal in order of excited electronic states from calculation thus implies that the vertical transitions LUMO ← HOMO − 1 and LUMO + 1 ← HOMO correspond to the observed $S_1 \leftarrow S_0$ transition. Our CIS calculation further reveals that the oscillator strength contains essentially equal contributions of the two L_b transitions. This is an extreme case of configuration interactions of nearly degenerate states.

The ambiguity in the order of electronic states is related to the size and class of the PAHs. In our previous studies of tetracene and pentacene,[31,43] the order of the excited states was unambiguous. The first excited state is almost a pure LUMO ← HOMO transition (L_a) along the short axis, the same as that from our calculation. Typically neutral PAHs have three absorption band systems: α, p, and β, as defined by Clar.[59] The L_a transition is the p-band in Clar's classification and the L_b transition is the α-band, much weaker than the p band. Empirically, with the growing size of the aromatic molecule, both p- and α-bands shift to the red, but the two transitions shift at different rates depending on the detailed molecular structure, and the resulting order of states adjusts accordingly.

TABLE 3: Molecular Geometry Parameters of Pyrene in the S_0, S_1, and D_0 States

	S_0			
	calculation	experiment[60]	S_1	D_0
		Bond Length (Å)		
C1−C2	1.39131	1.395	1.39462	1.39018
C2−C3	1.40210	1.406	1.39714	1.42101
C3−C4	1.43629	1.438	1.41948	1.41614
C4−C5	1.35848	1.367	1.36252	1.38221
C15−C16	1.42485	1.425	1.37626	1.41461
C3−C15	1.42633	1.430	1.44541	1.42262
		Distance (Å)		
C4−C12	4.92126		4.90918	4.89357
C1−C8	7.03643		7.02547	7.06780

Geometry and Vibrational Modes of the S_1 State. By setting the control key to root = 2 in the CIS/6-311G(d,p) calculation for the $^1B_{2u}$ state, the resulting geometry parameters for the S_1 state are listed in Table 3. In addition to our calculation result, the parameters from neutron diffraction of pyrene crystals are also listed in Table 3 for the S_0 state.[60] Upon excitation to the S_1 state, the most notable change is the shortened bond of C15−C16. From Figure 4, in the transition of LUMO ← HOMO − 1, the antibonding character between C15 and C16 in HOMO − 1 should be attenuated by the additional horizontal nodal plane in the LUMO, whereas in the transition of LUMO + 1 ← HOMO, the additional bonding character in the LUMO + 1 between C15 and C16 should shrink the bond length upon excitation. It is interesting to also note that regardless of the changes in nodal planes, the overall size of the molecular frame remains similar upon electronic excitation and even ionization. This fact manifests the ability of the aromatic system in accommodating variations in electron density and charge.

Two other bonds are also affected by the electronic transition, although to a much lesser degree than that of C15 − C16. The bond length of C3 − C4 is shortened, whereas that of C3 − C15 is lengthened. The latter result is understandable for the LUMO + 1 ← HOMO transition, with the addition of a nodal plane between C3 and C15. The C3 − C4 bond should be strengthened somewhat in the LUMO ← HOMO − 1 transition because of the higher electron density on C4 in the LUMO. In the meantime, its antibonding character should be attenuated in the LUMO + 1 because of the lower electron density on C4.

The changes in bond length are in agreement with the observed vibrational modes in the REMPI spectrum of Figure 1. We performed a Franck−Condon calculation[61,62] for the $S_1 \leftarrow S_0$ transition using the program from Dr. Dongsheng Yang, and the resulting Franck−Condon factors for transitions to modes 13−11 are 5:7:1. This ratio underestimates the intensity of mode 11, but for modes 13 and 12, it is qualitatively correct.

Geometry and Vibrational Modes of the D_0 State. In the $D_0 \leftarrow S_1$ transition, an electron is removed from S_1 and the final cation geometry should only be affected by the final electron configuration. Because the HOMO and HOMO − 1 are nearly degenerate, and the final ionic state has an odd number of

electrons, a Jahn−Teller-like effect might result in a larger separation in energies between the two orbitals, thereby resulting in a single electron configuration. This speculation agrees with the changes in the calculated bond length from S_0 to D_0 as listed in Table 3. The overall molecular length in the vertical direction represented by C4−C12 is decreased, in agreement with the removal of an electron from an orbital with horizontal nodal planes, that is, the HOMO. In addition, the bond length of C3−C4 is shorter in D_0, in agreement with the fact that a nodal plane passes through the C3−C4 bond in the HOMO. On the other hand, the overall horizontal dimension of the molecule represented by C1−C8 is slightly larger in D_0, a result that could not be explained by the loss of an electron from the HOMO − 1. Elongations of both the C2−C3 and C4−C5 bonds are also contradictive to the removal of an electron from HOMO − 1. Thus, although the $S_1 \leftarrow S_0$ transition is essentially a complete mixture of two configurations in both the initial and final MOs, the electron configuration of the cation is almost exclusively $(\text{HOMO} - 1)^2(\text{HOMO})^1$.

To understand the observed vibrational modes in ZEKE, however, we need to consider both $(\text{HOMO} - 1)^2(\text{HOMO})^1 \leftarrow (\text{HOMO} - 1)^1(\text{HOMO})^2(\text{LUMO})^1$ and $(\text{HOMO} - 1)^2(\text{HOMO})^1 \leftarrow (\text{HOMO} - 1)^2(\text{HOMO})^1(\text{LUMO} + 1)^1$. The latter case is straightforward, involving only the removal of the LUMO + 1 electron. The decreased antibonding character in the vertical direction agrees with the activation of mode 12, that is, stretching in the vertical direction. The former case involving a LUMO electron is more complicated, and a two-step process is necessary to reach the final electron configuration $(\text{HOMO} - 1)^2(\text{HOMO})^1$. The removal of a horizontal nodal plane with the removal of the LUMO electron is also a mechanism of activating mode 12. Further relaxation for an electron from HOMO to HOMO − 1 involves changing all three vertical nodal planes into horizontal, a process essentially impossible to achieve due to the orthogonality of the two MOs. We therefore propose that ionization from the electron configuration $(\text{HOMO} - 1)^1(\text{HOMO})^2(\text{LUMO})^1$ does not lead to the ground cationic state D_0 and hence is not observable from the current ZEKE experiment.

The Mulliken charge distribution for the D_0 state is calculated with the Gaussian 03 suite. We placed the net charges on the peripheral hydrogen atoms to the adjacent ring, and divided the charges on the shared carbon atoms to the conjoint rings. About 60% of the positive charge is located on the rings along the long axis, while 40% is on the rings along the short axis. This charge distribution is complementary to the electron density distribution of the HOMO. The opposite is true for the HOMO − 1, with a much lower concentration of positive charges (about 30%) located on the longitudinal rings. This result is also supportive of our assessment of the single electron configuration $(\text{HOMO} - 1)^2(\text{HOMO})^1$ for the D_0 state. The unequal distribution of charges on the two unique types of rings can be largely attributed to the loss of electron density on carbons 2, 7, 9, and 14 upon ionization. This result is not surprising from the point of view of basic organic chemistry: these carbon atoms are known to be the most reactive and most likely sites for substitution reactions.

It is worth noting that no previous experimental information of pyrene cation is available in the frequency region below 500 cm^{-1}, largely due to practical difficulties in FIR spectroscopy. Thus even just for calibration and scaling purposes, ZEKE is of considerable value, particularly for predictions of IR active modes in the FIR region. Governed by the selection rule of ZEKE spectroscopy, no IR active mode has been observed in the current work. Consequently, we cannot make any comparisons with previous experimental and theoretical studies even in the region above 500 cm^{-1}.[23,37−40] This fact further manifests the complementary nature of ZEKE to other direct single photon processes such as matrix isolation spectroscopy or infrared multiphoton dissociation.

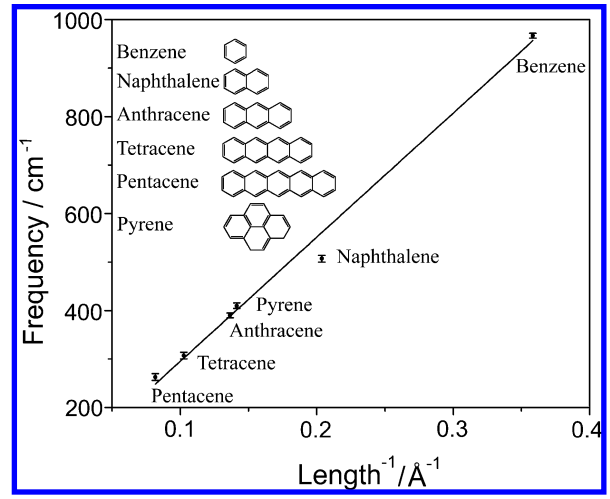

Figure 5. Frequencies of the longitudinal stretching mode vs the reciprocal length of a PAH molecule including benzene, naphthalene, anthracene, tetracene, pentacene, and pyrene.[31,41−43,63] The error bars are reported experimental uncertainties.

Comparisons with Cata-Condensed PAHs. On the basis of our study of cata-condensed PAHs of tetracene and pentacene,[31,43] the frequency of the a_g longitudinal stretching mode shifts to lower values with the increase of the number of aromatic rings. The longitudinal dimension of the carbon skeleton and the observed frequencies of the longitudinal stretching mode for a few PAHs are plotted in Figure 5. The error bars in the figure represent reported experimental uncertainties.[31,41−43,63] All listed PAHs have D_{2h} symmetry except for benzene, which has D_{6h} symmetry. A least-squares regression of the data points in Figure 5 reveals a reciprocal relationship between the frequency and the molecular length, with a R^2 of 0.9918. The trend of red shift is thus not limited to cata-condensed PAHs, and the peri-condensed pyrene is no exception. It would be interesting to expand the current investigation to other peri-condensed PAHs for further in-depth studies.

The observation of the b_{2g} out-of-plane waving modes 41 and 39 of pyrene implies some degree of corrugation of the molecular plane. In the polyacene series, this type of out-of-plane waving mode was only observed in pentacene.[31] Although the length of pyrene is close to but slightly smaller than that of anthracene, the expansion of the molecular frame in the orthogonal direction seems to offer extra flexibility in the molecular frame, allowing the activation of the b_{2g} modes along both the long and short axes.

Typically DFT calculations provide reliable vibrational frequency information for the cation, as demonstrated in our own work on cata-condensed PAHs and a series of small benzene derivatives.[31,43,52−56] In the case of pyrene, the maximum deviation is ~21 cm^{-1} without any scaling factor. The scaling factor of 0.995 further reduces the deviation to 17 cm^{-1}. This level of agreement is less than impressive. In addition, as mentioned in our previous publication,[31] the agreement between experiment and theory in ZEKE intensity based on Franck−Condon factors is still qualitatively unsatisfactory. Reliability in theoretical calculations for the ground state of the cation is

crucial for astrophysical modeling, since IR active modes not typically observable in ZEKE play important roles for spectroscopic surveys and modeling of energy and chemical balances in the universe. The current results further illustrate the need for experimental data, both in terms of astrophysical modeling and further improvements in DFT calculations.

Conclusion

Spectroscopic properties of the electronically excited and ionic states of pyrene have been studied using $1 + 1'$ two-color REMPI and two-color ZEKE. Although the small peri-condensed PAH is not expected to have pronounced nonrigidity, pyrene shows the character of large PAHs in both the nature of the electronic transition and vibronic coupling. The first excited electronic state is L_b in nature, and vibronic bands due to Herzberg−Teller coupling are only slightly weaker in intensity than those of Franck−Condon allowed a_g modes. Unique to the peri-condensed PAHs, some of the observed out-of-plane waving modes have a two-dimensional evolution pattern, spreading in both directions of the molecular plane. For the Franck−Condon allowed a_g mode corresponding to longitudinal stretching of the molecular frame, we have established a close correlation between frequency and molecular shape and size, and this information can assist with astrophysical studies of PAH related subjects.

Simple Hückel calculations offer a simplistic view of the related MOs and distribution of nodal planes. This type of qualitative information is helpful in understanding the change in geometry and activation of vibrational modes upon electronic excitation and ionization. However, even with CIS and TDDFT, the order of the excited electronic state from calculation is still questionable, and near degeneracy of MOs and electronic states due to high symmetry should serve as a warning in the interpretation of theoretical results. The extensive configuration interaction in the first two electronically excited states of pyrene is expected to persist for larger PAHs with similar symmetry, and detailed analysis of vibrational and polarization spectroscopy is necessary for the symmetry assignment of the related electronic states.

Acknowledgment. This work is supported by the National Aeronautics and Space Administration under award No. NNX09AC03G. Acknowledgment is made to the donors of The Petroleum Research Fund, administered by the American Chemical Society, for partial support of this research.

References and Notes

(1) Parr, R. *The Quantum Theory of Molecular Electronic Structure*; W. A. Benjamin: New York, 1964.
(2) Sami, S.; Faisal, M.; Huggett, R. J. *Mar. Biol.* **1992**, *113*, 247–252.
(3) Smith, L. E.; Denissenko, M. F.; Bennett, W. P.; Li, H.; Amin, S.; Tang, M.-S.; Pfeifer, G. P. *J. Natl. Cancer Inst.* **2000**, *92*, 803–811.
(4) Kriek, E.; Rojas, M.; Alexandrov, K.; Bartsch, H. *Mutat. Res. Fundam. Mol. Mech. Mugag.* **1998**, *400*, 215–231.
(5) Harvey, R. G. *Polycyclic Aromatic Hydrocarbons: Chemistry and Carcinogenicity*; Cambridge University Press: London, 1991.
(6) Baude, P. F.; Ender, D. A.; Haase, M. A.; Kelley, T. W.; Muyres, D. V.; Theiss, S. D. *Appl. Phys. Lett.* **2003**, *82*, 3964–3966.
(7) Knipp, D.; Street, R. A.; Völkel, A.; Ho, J. *J. Appl. Phys.* **2003**, *93*, 347–355.
(8) Bréchignac, P.; Pino, T.; Boudin, N. *Spectrochim. Acta, Part A* **2001**, *57*, 745–756.
(9) Salama, F.; Galazutdinov, G. A.; Krełowski, J.; Allamandola, L. J.; Musaev, F. A. *Astrophys. J.* **1999**, *526*, 265–273.
(10) Bernstein, M. P.; Dworkin, J. P.; Sandford, S. A.; Cooper, G. W.; Allamandola, L. J. *Nature* **2002**, *416*, 401–403.
(11) Wakeham, S. G.; Schaffner, C.; Giger, W. *Geochim. Cosmochim. Acta* **1980**, *44*, 415–429.
(12) Shock, E. L.; Schulte, M. D. *Nature* **1990**, *343*, 728–731.
(13) Allamandola, L. J.; Tielens, A. G. G. M.; Barker, J. R. *Astrophys. J.* **1985**, *290*, L25–L28.
(14) Léger, A.; Puget, J. L. *Astron. Astrophys.* **1984**, *137*, L5–L8.
(15) Malloci, G.; Mulas, G.; Benvenuti, P. *Astron. Astrophys.* **2003**, *410*, 623–637.
(16) Mulas, G.; Malloci, G.; Benvenuti, P. *Astron. Astrophys.* **2003**, *410*, 639–648.
(17) Peeters, E.; Allamandola, L. J.; Hudgins, D. M.; Hony, S.; Tielens, A. G. G. M. *Astron. Soc. Pac. Conf. Ser.* **2004**, *309*, 141–162.
(18) Li, A. PAHs in comets: An overview. In *Deep Impact As a World Observatory Event: Synergies in Space, Time, and Wavelength*; Kaufl, H. U., Siebenmorgen, R., Moorwood, A. F. M., Eds.; Springer: Berlin, 2009; pp 161−175.
(19) Rhee, Y. M.; Lee, T. J.; Gudipati, M. S.; Allamandola, L. J.; Head-Gordon, M. *Proc. Natl. Acad. Sci.U. S. A.* **2007**, *104*, 5274–5278.
(20) Langhoff, S. R. *J. Phys. Chem.* **1996**, *100*, 2819–2841.
(21) Zhang, K.; Guo, B.; Colarusso, P.; Bernath, P. F. *Science* **1996**, *274*, 582–583.
(22) Joblin, C.; Berné, O.; Simon, A.; Mulas, G. arXiv:0904.3185 2009.
(23) Hudgins, D. M.; Allamandola, L. J. *J. Phys. Chem.* **1995**, *99*, 3033–3046.
(24) Hudgins, D. M.; Allamandola, L. J. *J. Phys. Chem.* **1995**, *99*, 8978–8986.
(25) Hudgins, D. M.; Allamandola, L. J. *J. Phys. Chem. A* **1997**, *101*, 3472–3477.
(26) Hudgins, D. M.; Sandford, S. A. *J. Phys. Chem. A* **1998**, *102*, 353–360.
(27) Hudgins, D. M.; Sandford, S. A. *J. Phys. Chem. A* **1998**, *102*, 344–352.
(28) Hudgins, D. M.; Sandford, S. A. *J. Phys. Chem. A* **1998**, *102*, 329–343.
(29) Parisel, O.; Berthier, G.; Ellinger, Y. *Astron. Astrophys.* **1992**, *266*, L1–L4.
(30) Schlag, E. W. *ZEKE spectroscopy*; Cambridge University Press: London, 1998.
(31) Zhang, J.; Han, F.; Pei, L.; Kong, W.; Li, A. *Astrophys. J.* **2010**, *715*, 485–492.
(32) Draine, B. T.; Li, A. *Astrophys. J.* **2001**, *551*, 807–824.
(33) Draine, B. T.; Li, A. *Astrophys. J.* **2007**, *657*, 810–837.
(34) Li, A.; Draine, B. T. *Astrophys. J.* **2001**, *554*, 778–802.
(35) Li, A.; Draine, B. T. *Astrophys. J.* **2002**, *576*, 762–772.
(36) Li, A.; Lunine, J. I. *Astrophys. J.* **2003**, *594*, 987–1010.
(37) Oomens, J.; Van Roij, A. J. A.; Meijer, G.; von Helden, G. *Astrophys. J.* **2000**, *542*, 404–410.
(38) Szczepanski, J.; Vala, M. *Astrophys. J.* **1993**, *414*, 645–655.
(39) Kim, H. S.; Wagner, D. R.; Saykally, R. J. *Phys. Rev. Lett.* **2001**, *86*, 5691.
(40) Vala, M.; Szczepanski, J.; Pauzat, F.; Parisel, O.; Talbi, D.; Ellinger, Y. *J. Phys. Chem.* **1994**, *98*, 9187–9196m.
(41) Cockett, M. C. R.; Kimura, K. *J. Chem. Phys.* **1994**, *100*, 3429–3441.
(42) Cockett, M. C. R.; Ozeki, H.; Okuyama, K.; Kimura, K. *J. Chem. Phys.* **1993**, *98*, 7763–7772.
(43) Zhang, J.; Pei, L.; Kong, W. *J. Chem. Phys.* **2008**, *128*, 104301.
(44) Mangle, E. A.; Topp, M. R. *J. Phys. Chem.* **1986**, *90*, 802–807.
(45) Borisevich, N. A.; Vodovatov, L. B.; D'yachenko, G. G.; Petukhov, V. A.; Semyonov, M. A. *J. Appl. Spectrosc.* **1995**, *62*, 482–488.
(46) Dierksen, M.; Grimme, S. *J. Chem. Phys.* **2004**, *120*, 3544–3554.
(47) Baba, M.; Saitoh, M.; Kowaka, Y.; Taguma, K.; Yoshida, K.; Semba, Y.; Kasahara, S.; Yamanaka, T.; Ohshima, Y.; Hsu, Y.-C.; Lin, S. H. *J. Chem. Phys.* **2009**, *131*, 224318.
(48) Tanaka, J. *Bull. Chem. Soc. Jpn.* **1965**, *38*, 86–102.
(49) Bito, Y.; Shida, N.; Toru, T. *Chem. Phys. Lett.* **2000**, *328*, 310–315.
(50) Joblin, C.; d'Hendecourt, L.; Léger, A.; Défourneau, D. *Astron. Astrophys.* **1994**, *281*, 923–936.
(51) Frisch, M. J.; Trucks, G. W.; Schlegel, H. B.; Scuseria, G. E.; Robb, M. A.; Cheeseman, J. R.; Montgomery, Jr., J. A.; Vreven, T.; Kudin, K. N.; Burant, J. C.; Millam, J. M.; Iyengar, S. S.; Tomasi, J.; Barone, V.; Mennucci, B.; Cossi, M.; Scalmani, G.; Rega, N.; Petersson, G. A.; Nakatsuji, H.; Hada, M.; Ehara, M.; Toyota, K.; Fukuda, R.; Hasegawa, J.; Ishida, M.; Nakajima, T.; Honda, Y.; Kitao, O.; Nakai, H.; Klene, M.; Li, X.; Knox, J. E.; Hratchian, H. P.; Cross, J. B.; Bakken, V.; Adamo, C.; Jaramillo, J.; Gomperts, R.; Stratmann, R. E.; Yazyev, O.; Austin, A. J.; Cammi, R.; Pomelli, C.; Ochterski, J. W.; Ayala, P. Y.; Morokuma, K.; Voth, G. A.; Salvador, P.; Dannenberg, J. J.; Zakrzewski, V. G.; Dapprich, S.; Daniels, A. D.; Strain, M. C.; Farkas, O.; Malick, D. K.; Rabuck, A. D.; Raghavachari, K.; Foresman, J. B.; Ortiz, J. V.; Cui, Q.; Baboul, A. G.; Clifford, S.; Cioslowski, J.; Stefanov, B. B.; Liu, G.; Liashenko, A.; Piskorz, P.; Komaromi, I.; Martin, R. L.; Fox, D. J.; Keith, T.; Al-Laham, M. A.; Peng, C. Y.; Nanayakkara, A.; Challacombe, M.; Gill, P. M. W.; Johnson,

B.; Chen, W.; Wong, M. W.; Gonzalez, C.; and Pople, J. A. *Gaussian 03, Revision E.01*; Gaussian, Inc.: Wallingford CT, 2004.

(52) He, Y.; Wu, C.; Kong, W. *J. Chem. Phys.* **2004**, *121*, 8321–8328.

(53) He, Y.; Wu, C.; Kong, W. *Chem. Phys. Lett.* **2004**, *391*, 38–43.

(54) He, Y.; Wu, C.; Kong, W. *J. Chem. Phys.* **2004**, *121*, 3533–3539.

(55) Wu, C.; He, Y.; Kong, W. *Chem. Phys. Lett.* **2004**, *398*, 351–356.

(56) He, Y.; Kong, W. *J. Chem. Phys.* **2006**, *124*, 2043061.

(57) Hager, J. W.; Wallace, S. C. *Anal. Chem.* **1988**, *60*, 5–10.

(58) Callis, P. R.; Scott, T. W.; Albrecht, A. C. *J. Chem. Phys.* **1983**, *78*, 16–22.

(59) Clar, E. *Polycyclic Hydrocarbons*; Academic Press: London, 1964.

(60) Hazell, A. C.; Larsen, F. K.; Lehmann, M. S. *Acta Crystallogr., Sect. B: Struct. Crystallogr. Cryst. Chem.* **1972**, *28*, 2977–2984.

(61) Berces, A.; Zgierski, M. Z.; Yang, D.-S. *Computational Molecular Spectroscopy*; John Wiley & Sons: New York, 2000.

(62) Yang, D.-S.; Zgierski, M. Z.; Rayner, D. M.; Hackett, P. A.; Martinez, A.; Salahub, D. R.; Roy, P.-N.; Carrington, T. *J. Chem. Phys.* **1995**, *103*, 5335–5342.

(63) Kwon, C. H.; Kim, H. L.; Kim, M. S. *J. Chem. Phys.* **2003**, *119*, 215–223.

JP1024813